ISAC Antenna Topologies Study Ranging from Massive to Cell-Free MIMO

Kaitao Meng*, Kawon Han*, and Christos Masouros*
*Department of Electronic and Electrical Engineering, University College London, UK
Emails: *{kaitao.meng, kawon.han c.masouros}@ucl.ac.uk

***Abstract*—We propose a cooperative integrated sensing and communication (ISAC) architecture that integrates coordinated multi-point (CoMP) communication with multi-static sensing. Our work examines the impact of antenna-to-base stations (BSs) allocation on both sensing and communication performance. To this end, we contrast the benefits of concentrated antennas, boosting beamforming and coherent processing in massive MIMO systems, with those of distributed antennas, which improve diversity and shorten access distances in cell-free setups. For sensing, we assess two localization methods, including AOA-based, TOF-based, to determine their effects on network performance. In terms of communication, our results indicate that higher path loss exponents favor distributed configurations, while lower exponents benefit centralized setups. Simulations confirm that our cooperative scheme outperforms non-cooperative approaches, surpassing purely centralized or distributed strategies.**

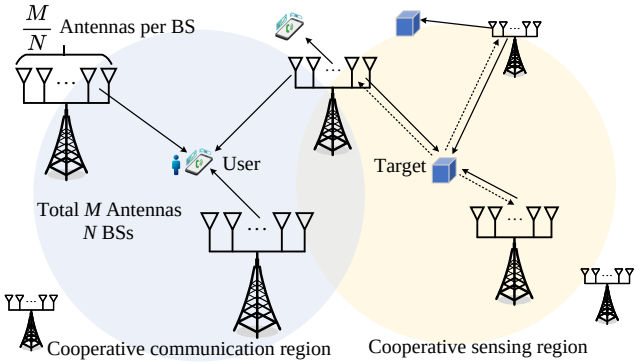

Fig. 1. Illustration of antenna-to-BS allocation in cooperative ISAC networks with optimized BS density (Blue line refers to other time-frequency resources).

I. Introduction

Given rising spectrum scarcity and interference issues between separate sensing and communication (S&C) systems, integrated sensing and communication (ISAC) has attracted significant academic and industrial interest [1]. ISAC leverages unified infrastructure and waveforms to simultaneously transmit information and receive echoes, thereby enhancing spectrum, cost, and energy efficiency [2]. Owing to the limited coverage of link-level ISAC, network-level ISAC, especially multi-cell S&C cooperation, has received increased focus [3].

Network-level ISAC offers expanded coverage, improved service quality, flexible performance tradeoffs, and richer target information [4]. By exploiting both monostatic (BS-to-target-to-originating BS) and bistatic (BS-to-target-to-other BSs) links, cooperative BSs can maximize sensing capabilities. Moreover, coordinated multi-point (CoMP) techniques mitigate inter-cell interference and boost communication by linking a user to multiple BSs for enhanced reliability and throughput [5]. Although prior studies have examined network-level S&C tradeoffs through waveform design and cluster optimization [6], [7], few have addressed how antenna topology influences overall performance.

Optimal antenna-to-BS allocation, defined by the number of antennas per site, is crucial for maximizing cooperative gains, as sensing and communication have different configuration requirements. Generally, allocation strategies are categorized as centralized or distributed. Centralized MIMO systems concentrate antennas at one site to simplify deployment and reduce costs, as in conventional cellular networks [8]. In contrast, distributed MIMO (e.g., cell-free systems) disperses antennas to mitigate channel correlation, enhance spatial diversity, and shorten access distances [9].

We propose a cooperative ISAC scheme that merges centralized and distributed strategies to balance beamforming gain and geometric diversity. Specifically, concentrating antennas boosts beamforming and coherent processing can reduce BS density and increases service distance, whereas distributing antennas improves sensing and communication over shorter distances. While some work has optimized antenna configurations based on specific user or target locations [10], practical uncertainties in user, target, and BS positions, as well as channel fading, require robust allocation strategies.

As shown in Fig. 1, in the proposed scheme, multiple BSs within a communication region jointly transmit the same data, while another set collaborates on target localization. By integrating CoMP-based joint transmission with multi-static sensing, our approach achieves a balance between sensing and communication at the network level. We evaluate two localization methods, AOA-based and TOF-based, to assess the impact of antenna-to-BS allocation on network performance, revealing the following scaling laws: TOF-based methods scale as $\ln^2 N$, and AOA-based as $\ln N$. For communication, determination of optimal antenna-to-BS allocation shows that larger path loss exponents favor distributed configurations to reduce access distances, whereas smaller exponents favor centralized setups to maximize beamforming gain. A performance boundary optimization demonstrates that cooperative transmission and sensing can effectively improve S&C gains while offering a flexible tradeoff between the two functionalities.

II. System Model

As shown in Fig. 1, BSs within a circle of radius D (centered at the target/user) form a cooperative cluster. For communication, these BSs use CoMP by transmitting identical signals to enhance received power via constructive superposition. For target localization, they operate as a distributed multi-static MIMO radar employing code-division multiplexing to ensure waveform orthogonality. Due to the cost and complexity of phase-level synchronization, our design opts for non-coherent joint transmission and non-coherent MIMO radar processing, balancing performance and feasibility. This study explores optimal antenna allocation in cooperative ISAC networks under fixed total antenna resources. While centralized arrays boost beamforming and coherent gains, distributing antennas improves macro-multiplexing and spatial diversity. Our scheme thus navigates the tradeoff among coherent gain, macro-multiplexing, and geometric diversity.

With a fixed total number of antennas of the given region, i.e., fixed antenna density, we optimize the antenna number per BS, as shown Fig. 1. Define antenna density as antennas per km^2 and BS density as BSs per km^2. Given transmit and receive antenna densities λ_t and λ_r, and assuming each BS employs a uniform linear array, the BS density is $\lambda_b = \frac{\lambda_t}{M_t} = \frac{\lambda_r}{M_r}$, where M_t and M_r represent the number of transmit and receive antennas per BS, respectively. Assuming a fixed overall antenna density, increasing the number of antennas per BS inevitably reduces the total BS density. We model the BS locations as a homogeneous Poisson point process (PPP) in a two-dimensional space, represented by $\Phi_b = \{\mathbf{d}_i = [x_i, y_i]^T \in \mathbb{R}^2 : i \in \mathbb{N}^+\}$, where each $\mathbf{d}_i$ specifies the position of BS i.

Each BS employs transmit precoding (TPC) to simultaneously deliver the information signal $s^c(t)$ to its served user and a dedicated radar signal $s_i^s(t)$ for target localization, where t denotes the time instant. We assume that $\mathrm{E}[s_i^s(t)(s_i^c)^H(t)] = 0$. For simplicity, the time argument (t) is omitted from the S&C signal notation in the following discussion. By defining $\mathbf{s}_i = [s_i^s, s_i^c]^T$, we obtain $\mathrm{E}\left[\mathbf{s}_i\mathbf{s}_i^H\right] = \mathbf{I}_2$. Then, the signal transmitted by the ith BS is given by

$$\mathbf{x}_i = \mathbf{W}_i\mathbf{s}_i = \mathbf{w}_i^c s_i^c + \mathbf{w}_i^s s_i^s, \tag{1}$$

where $\mathbf{w}_i^c$ and $\mathbf{w}_i^s \in \mathbb{C}^{M_\mathrm{t}\times 1}$ are TPC vectors, with $\|\mathbf{w}_i^c\|^2 = p^c$ and $\|\mathbf{w}_i^s\|^2 = p^s$. Here, p^s and p^c denote the transmit power allocated to the sensing and communication signals, respectively, and $\mathbf{W}_i = [\mathbf{w}_i^c, \mathbf{w}_i^s] \in \mathbb{C}^{M_\mathrm{t}\times 2}$ represents the TPC matrix for the BS located at $\mathbf{d}_i$. To eliminate interference between the S&C functions and simplify the analysis, we employ zero-forcing (ZF) beamforming. Then, the beamforming matrix of the serving BS i is given by $\mathbf{W}_i = \tilde{\mathbf{W}}_i \left(\sqrt{\mathrm{diag}\left(\tilde{\mathbf{W}}_i^H\tilde{\mathbf{W}}_i\right)}\right)^{-1}$, where $\tilde{\mathbf{W}}_i = \mathbf{H}_i\left(\mathbf{H}_i^H\mathbf{H}_i\right)^{-1}$ and $\mathbf{H}_i = [(\mathbf{h}_{i,c}^H)^T, (\mathbf{a}^H(\theta_i))^T]^T$. Here, $\mathbf{h}_{i,c}^H \in C^{M_\mathrm{t}\times 1}$ denotes the communication channel spanning from BS i to the typical user, and $\mathbf{a}^H(\theta_i) \in C^{M_\mathrm{t}\times 1}$ represents the sensing channel impinging from BS i to the typical target. We have $p^s + p^c = 1$ with normalized transmit power.

A. Cooperative Sensing Model

We investigate the optimal antenna-to-BS allocation by analyzing the scaling behavior of target localization techniques based on AOA measurements, TOF measurements, and their combination. Assuming unbiased estimates, the CRLB provides a theoretical benchmark for localization accuracy measured in mean squared error (MSE). A typical target is collaboratively sensed by N BSs, and we assume that the radar signals $\{s_i^s\}_{i=1}^N$ transmitted by the BSs in the cooperative sensing cluster are approximately orthogonal for any time delay of interest [11]. The base-band equivalent signal impinging on receiver j is expressed as

$$\mathbf{y}_j(t) = \sum\nolimits_{i=1}^{N} \sigma d_j^{-\frac{\beta}{2}} \mathbf{b}(\theta_j)\, d_i^{-\frac{\beta}{2}} \mathbf{a}^H(\theta_i)\mathbf{W}_i\boldsymbol{s}_i(t-\tau_{i,j}) + \mathbf{n}_l(t), \tag{2}$$

where $d_i = \|\mathbf{d}_i\|$ represents the distance from BS i to the origin, and $\beta \geq 2$ is the pathloss exponent between the serving BS and the typical target. Moreover, σ denotes the radar cross section (RCS), $\tau_{i,j}$ is the propagation delay for the link from BS i to the target and then to BS j. The term $\mathbf{n}_l(t)$ is the additive complex Gaussian noise with zero mean and covariance matrix $\sigma_s^2\mathbf{I}_{M_\mathrm{r}}$. Additionally, the steering vector is given by $\mathbf{a}^H(\theta_i) = [1, \cdots, e^{j\pi(M_\mathrm{t}-1)\cos(\theta_i)}]$, and the receiver response vector is $\mathbf{b}(\theta_j) = [1, \cdots, e^{j\pi(M_\mathrm{r}-1)\cos(\theta_j)}]^T$, where θ_i denotes the bearing angle from BS i to the target with respect to the horizontal axis. The cooperative sensing model ignores interference from echoes of other targets since distinct spatial positions, angles, and propagation delays enable advanced filtering techniques, such as adaptive filtering.

1) AOA Measurement based Localization: For the AOA estimate at the receiver j, the covariance matrix can be given by $\mathbf{R}_y = \mathbb{E}\left\{\mathbf{y}_j(t)\mathbf{y}_j^H(t)\right\}$, and perform an eigen-decomposition to separate the signal and noise subspaces. The MUSIC algorithm can be applied to this decomposition to generate a pseudospectrum, where the peak corresponds to the estimated AOA [12]. By measuring the AOAs of each monostatic link and bi-static link, the target location can be estimated by maximum likelihood estimation (MLE) [13]. The location of a typical target is denoted as $\boldsymbol{\psi}_t = [x_t, y_t]^T$. For the AOA measurement of the bi-static link from the jth BS to the target and then to the ith BS, we have

$$\hat{\theta}_{i,j} = \tan^{-1}\frac{y_t - y_i}{x_t - x_i} + n_{i,j}^a. \tag{3}$$

In (3), $n_{i,j}^a$ denotes the AOA measurement error, and $n_{i,j}^a \sim \mathcal{N}\left(0, \rho_{i,j}^2\right)$, where $\rho_{i,j}^2 = \frac{6}{\pi^2\cos^2\theta_i M_r(M_r^2-1)G_t\gamma_{i,j}}$ [14] and $\gamma_{i,j} = \frac{\sigma p^s\gamma_0}{d_i^\beta d_j^\beta}$. Here, G_t is the TPC gain, and γ_0 represents the channel power at the reference distance of 1 m. Then, we transform N^2 AOA measurement links into the target location. The Jacobian matrices of the N BS measurement errors, evaluated at the true target position $\boldsymbol{\psi}_t = [x_t, y_t]^T$, indicate

$$\mathbf{J}_\mathrm{A} = \begin{bmatrix} \frac{\partial\hat{\theta}_1}{\partial x_t} & \frac{\partial\hat{\theta}_1}{\partial y_t} \\ \vdots & \vdots \\ \frac{\partial\hat{\theta}_N}{\partial x_t} & \frac{\partial\hat{\theta}_N}{\partial y_t} \end{bmatrix} = \begin{bmatrix} \frac{-\sin\theta_1}{d_1} & \frac{\cos\theta_1}{d_1} \\ \vdots & \vdots \\ \frac{-\sin\theta_N}{d_N} & \frac{\cos\theta_N}{d_N} \end{bmatrix}_{N\times 2}. \tag{4}$$

Then, the Fisher information matrix (FIM) of estimating the target location for the AOA-based MIMO radar considered is equal to

$$\begin{aligned}\mathbf{F}_{\mathrm{A}} =& \tilde{\mathbf{J}}_{\mathrm{A}}^{T}\boldsymbol{\Sigma}_{\mathrm{A}}^{-1}\tilde{\mathbf{J}}_{\mathrm{A}} \\ =& |\zeta_a|^2 \sum\nolimits_{j=1}^{N}\sum\nolimits_{i=1}^{N}\frac{\cos^2\theta_i}{d_j^2 d_i^2}\begin{bmatrix} \frac{\sin^2\theta_i}{d_i^2} & -\frac{\sin\theta_i\cos\theta_i}{d_i^2} \\ -\frac{\sin\theta_i\cos\theta_i}{d_i^2} & \frac{\cos^2\theta_i}{d_i^2}\end{bmatrix},\end{aligned} \tag{5}$$

where $\tilde{\mathbf{J}}_{\mathrm{A}} = \left[\mathbf{J}_{\mathrm{A}}^{T},\cdots,\mathbf{J}_{\mathrm{A}}^{T}\right]^{T} \in \mathbb{C}^{N^2\times 2}$, $\boldsymbol{\Sigma}_{\mathrm{A}} = \mathrm{diag}(\rho_{1,1}^2,\cdots,\rho_{i,j}^2,\cdots,\rho_{N,N}^2) \in \mathbb{C}^{N^2\times N^2}$, and $|\zeta_a|^2 = \frac{1}{6}\pi^2 M_r\left(M_r^2-1\right)G_t\sigma p^s\gamma_0/\sigma_s^2$ [15]. Given the random location of ISAC BSs, the expected CRLB for any unbiased estimator of the target position is given by

$$\mathrm{CRLB}_{\mathrm{A}} = \mathrm{E}_{\Phi_b,G_t}\left[\mathrm{tr}\left(\mathbf{F}_{\mathrm{A}}^{-1}\right)\right]. \tag{6}$$

In (6), the expectation encompasses both the randomness of the BS locations and the variations in received beam power due to user channel fluctuations, thereby yielding the network's average sensing performance bound.

2) TOF Measurement based Localization: From transmitter j to the target and then to receiver i, the distance d_{ij} between the jth transmitter and the ith receiver is modeled as

$$\hat{d}_{ij}(\tau_{ij}) = d_{ij} + n_{ij}^r,$$

where $n_{ij}^r \sim \mathcal{N}\left(0,\eta_{ij}^2\right)$ and $\eta_{ij}^2 = \frac{3c^2\sigma_s^2}{2\pi^2 G_t M_r B^2\gamma_{ij}}$. Here, c represents the speed of light, and B^2 indicates the squared effective bandwidth, implying that a larger bandwidth results in a more precise TOF estimation. To estimate the range $\hat{d}_{ij}$ based on TOF, we apply matched filtering to the received signal by correlating it with a replica of the transmitted waveform. This procedure accentuates peaks associated with target-induced time delays, which are subsequently converted into range estimates using the speed of light. For signals emanating from transmitter i, the Jacobian matrices corresponding to the measurement errors at the N receivers, evaluated at the target position, are given by

$$\mathbf{J}_{\mathrm{R}}^{T} = \begin{bmatrix} \frac{\partial d_{11}}{\partial x_t} & \cdots & \frac{\partial d_{ij}}{\partial x_t} & \cdots & \frac{\partial d_{NN}}{\partial x_t} \\ \frac{\partial d_{11}}{\partial y_t} & \cdots & \frac{\partial d_{ij}}{\partial y_t} & \cdots & \frac{\partial d_{NN}}{\partial y_t}\end{bmatrix}, \tag{7}$$

where $\frac{\partial d_{ij}}{\partial x_t} = \cos\theta_i + \cos\theta_j$ and $\frac{\partial d_{ij}}{\partial y_t} = \sin\theta_i + \sin\theta_j$. Let $a_{ij} = \cos\theta_i + \cos\theta_j$ and $b_{ij} = \sin\theta_i + \sin\theta_j$. Then, the FIM of estimating the parameter vector $\boldsymbol{\psi}_t$ for the TOF measurement radar considered is equal to [16]

$$\begin{aligned}\mathbf{F}_{\mathrm{R}} =& \mathbf{J}_{\mathrm{R}}^{T}\boldsymbol{\Sigma}_{\mathrm{R}}^{-1}\mathbf{J}_{\mathrm{R}} \\ =& |\zeta_r|^2 \sum\nolimits_{i=1}^{N}\sum\nolimits_{j=1}^{N} d_i^{-\beta} d_j^{-\beta}\begin{bmatrix} a_{ij}^2 & a_{ij}b_{ij} \\ a_{ij}b_{ij} & b_{ij}^2\end{bmatrix},\end{aligned} \tag{8}$$

where $\boldsymbol{\Sigma}_{\mathrm{R}} = \mathrm{diag}(\eta_{1,1}^2,\cdots,\eta_{i,j}^2,\cdots,\eta_{N,N}^2)$. In (8), we have [16]

$$|\zeta_r|^2 = \frac{8\pi^2 p^s G_t M_r B^2\sigma\gamma_0}{c^2\sigma_s^2}. \tag{9}$$

In (9), $|\zeta_r|$ is the common system gain term. Given the random location of ISAC BSs, the expected CRLB for any unbiased estimator of the target position is given by

$$\mathrm{CRLB}_{\mathrm{R}} = \mathrm{E}_{\Phi_b,G_t}\left[\mathrm{tr}\left(\mathbf{F}_{\mathrm{R}}^{-1}\right)\right]. \tag{10}$$

Similarly, the expectation encompasses both the randomness of the BS locations and the variations in received beam power.

B. Cooperative Communication Model

Transmitters employ non-coherent joint transmission, meaning that the useful signals are combined through power accumulation. In our work, we adopt a user-centric clustering method where the BS closest to the typical user invites neighboring BSs within a distance D to participate in cooperation. Consequently, the signal received at the typical user is expressed as

$$\begin{aligned} y_c =& \underbrace{\sum\nolimits_{i\in\Phi_c} d_i^{-\frac{\alpha}{2}}\mathbf{h}_i^H\mathbf{W}_i\mathbf{s}_1}_{\text{collaborative intended signal}} + \underbrace{\sum\nolimits_{j\in\{\Phi_b\setminus\Phi_c\}} d_j^{-\frac{\alpha}{2}}\mathbf{h}_j^H\mathbf{W}_j\mathbf{s}_j}_{\text{inter-cluster interference}} \\ &+ n_c,\end{aligned} \tag{11}$$

where $\alpha \geq 2$ is the pathloss exponent, $\mathbf{h}_i^H \sim \mathcal{CN}\left(0,\mathbf{I}_{M_{\mathrm{t}}}\right)$ is the channel vector of the link between the BS at $\mathbf{d}_i$ to the typical user, Φ_c is the cooperative BS set, and n_c denotes the noise. In our analysis, the noise impact is neglected because interference from outside the cooperation region overwhelmingly dominates. The evaluation is based on the signal-to-interference ratio (SIR) [17]. The SIR of the received signal at the typical user can be expressed as

$$\mathrm{SIR}_c = \frac{\sum\limits_{i\in\Phi_c} g_i d_i^{-\alpha}}{\sum\limits_{j\in\{\Phi_b\setminus\Phi_c\}} g_j d_j^{-\alpha}}, \tag{12}$$

where $g_i = p^c\left|\mathbf{h}_i^H\mathbf{w}_i^c\right|^2$ and $g_j = p^c\left|\mathbf{h}_j^H\mathbf{w}_j^c\right|^2 + p^s\left|\mathbf{h}_j^H\mathbf{w}_j^s\right|^2$. The average data rate of users is given by

$$R_c = \mathrm{E}_{\Phi_b,g_i}[\log(1+\mathrm{SIR}_c)]. \tag{13}$$

III. Sensing Performance Analysis

To simplify our analysis, we assume that the number of BSs within a distance D from each target is equal to the expected count given the PPP density.

A. Angle Measurement Based Localization

In this subsection, we derive the closed-form CRLB expression under the assumption of random locations of both the BSs and targets. We transform $\mathrm{CRLB}_{\mathrm{A}}$ into

$$\begin{aligned}&\mathrm{E}_{\theta,d}\left[\frac{\sum_{i=1}^{N}\frac{f_i^2}{d_i^4}}{\sum_{j=1}^{N}\frac{1}{d_j^2}\left(\sum_{i=1}^{N}\frac{e_i^2}{d_i^4}\sum_{i=1}^{N}\frac{f_i^2}{d_i^4} - \left(\sum_{i=1}^{N}\frac{1}{d_i^4}e_i f_i\right)^2\right)}\right] \\ =&\mathrm{E}_{\theta,d}\left[\frac{\sum_{i=1}^{N}\frac{f_i^2}{d_i^4}}{\sum_{j=1}^{N}\frac{1}{d_j^2}\left(\sum_{i=1}^{N}\sum_{i>j}^{N}\frac{1}{d_i^4 d_j^4}(X_{i,j})^2\right)}\right],\end{aligned} \tag{14}$$

where $X_{i,j} = \sin\theta_i\cos\theta_i\cos^2\theta_j - \sin\theta_j\cos\theta_j\cos^2\theta_i$, $e_i = \sin\theta_i\cos\theta_i$, and $f_i = \cos^2\theta_i$. When the number of nodes is large, the correlation between the numerator and the denominator becomes negligible, as the distances of different

nodes are statistically independent under a PPP distribution. Moreover, when the number of nodes is large, the variability of the denominator is relatively small compared to its expected value. Then, CRLB can be approximated as

$$\mathrm{CRLB_A} = \frac{16\sum_{i=1}^{N}\mathrm{E}[d_i]^{-\beta-2}}{3\sum_{k=1}^{N}\mathrm{E}[d_k]^{-\beta}\sum_{i=1}^{N}\sum_{i>j}^{N}\mathrm{E}[d_i]^{-\beta-2}\mathrm{E}[d_j]^{-\beta-2}}. \tag{15}$$

Furthermore, the expected distance from the nth closest BS to the typical target can be given by $E[d_n] = \frac{\Gamma\left(n+\frac{1}{2}\right)}{\sqrt{\lambda_b\pi}\Gamma(n)} \approx \sqrt{\frac{n}{\lambda_b\pi}}$. When $\beta = 2$, we have $\lim_{N\to\infty}\sum_{n=1}^{N}\frac{1}{n} \approx \ln N + \gamma + \frac{1}{2N}$ and $\lim_{N\to\infty}\sum_{n=1}^{N}\frac{1}{n^2} \approx \frac{\pi^2}{6}$, where $\gamma = 0.577$.

$$\begin{aligned}\mathrm{CRLB_A} \approx & \frac{\sum_{i=1}^{N} i^{-2}}{\frac{3}{32}\lambda_b^3\pi^3\left(\sum_{j=1}^{N} i^{-1}\right)\left(\left(\sum_{i=1}^{N} i^{-2}\right)^2 - \sum_{i=1}^{N} i^{-4}\right)} \\ \approx & \frac{320}{3\lambda_b^3\pi^5\left(\ln N + \gamma + \frac{1}{2N}\right)}.\end{aligned} \tag{16}$$

For optimal sensing performance, the transmit beamforming gain can be approximated as $\left\lfloor\frac{\lambda_t D^2\pi}{N}\right\rfloor$, and the BS density can be denoted by $\frac{N}{\pi D^2}$. Then, we have

$$\begin{aligned}\mathrm{CRLB_A} \approx & \frac{1}{|\tilde{\zeta}_a|^2\underbrace{\left\lfloor\frac{\lambda_r D^2\pi}{N}\right\rfloor^3}_{\text{Receive gain}}\underbrace{\left\lfloor\frac{\lambda_t D^2\pi}{N}\right\rfloor}_{\text{Transmit gain}}\underbrace{\frac{N^3}{(D^2\pi)^3}\pi^5\ln N}_{\text{Geometry gain}}} \\ \approx & \frac{320N}{3|\tilde{\zeta}_a|^2 D^2\pi^6\lambda_t\lambda_r\ln N},\end{aligned} \tag{17}$$

where $|\tilde{\zeta}_a|^2 = \frac{1}{6}\pi^2\sigma p^s\gamma_0/\sigma_s^2$. According to (17), as the number of BSs increases, the value of $\mathrm{CRLB_A}$ also increases monotonically with N. Therefore, under fixed total transmit power constraints, a fully distributed antenna allocation is unlikely to be optimal. This is primarily because accurate AOA measurement relies on multiple antennas to enhance estimation accuracy.

Additionally, we examine a practical scenario in which the total transmit power across the region is fixed, implying that the BS transmit power scales linearly with the number of antennas. Consequently, the beamforming gain increases quadratically with the number of antennas, and then the corresponding CRLB is

$$\mathrm{CRLB_A^{M_t}} \approx \frac{320N^2}{3|\tilde{\zeta}_a|^2 D^4\pi^7\lambda_t^2\lambda_r\ln N}. \tag{18}$$

It is clear that, whether the system operates under a fixed total transmit power or scales power based on the number of antennas, when $N \gg 1$, increasing the number of antenna locations (or BS density) while keeping the antenna density constant leads to a higher CRLB for the AOA-based localization method.

B. Range Measurement Based Localization

According to the derived scaling law in [6], for the fixed total transmit power constraints, we have

$$\mathrm{CRLB_R} \approx \frac{2}{|\tilde{\zeta}_r|^2 D^2\pi^2\lambda_t\lambda_r\ln^2 N}, \tag{19}$$

where $|\tilde{\zeta}_r|^2 = \frac{8\pi^2 p^s B^2\sigma\gamma_0}{c^2\sigma_s^2}$, According to (19), when the number of BSs is sufficiently large, the $\mathrm{CRLB_R}$ value decreases monotonically as the number of BSs N increases. Therefore, given the total BS power constraint, the TOF-based localization method tends to favor a distributed antenna allocation to achieve better sensing results at closer distances. Similarly, if the total power of each BS increases with M_t, we have

$$\mathrm{CRLB_R^{M_t}} \approx \frac{2N}{|\tilde{\zeta}_r|^2 D^4\pi^3\lambda_t^2\lambda_r\ln^2 N}. \tag{20}$$

IV. Communication Performance

To analyze the optimal antenna-to-BS allocation, we adopt simplifications for maximizing the expected SIR. First, we simplify the expected data rate as

$$\mathrm{E}_{r,\Phi_b^S,g_i}\left[\ln\left(1+\frac{S}{I}\right)\right] \approx \mathrm{E}_r\left[\ln\left(1+\frac{\bar{S}_r}{\bar{I}_r}\right)\right], \tag{21}$$

where $\bar{S}_r = \mathrm{E}_{\Phi_b,g_i}[g_1 + \sum_{i\in\Phi_a} g_i\left\|\mathbf{d}_i\right\|^{-\alpha} r^\alpha] = p^c r^{-\alpha} + \frac{\pi\lambda_b}{\alpha-2}\left(r^{-\alpha+2} - D^{-\alpha+2}\right)$ and $\bar{I}_r = \mathrm{E}_{\Phi_b,g_i}\left[\sum_{j\in\{\Phi_b\setminus\Phi_a\}} g_j\left\|\mathbf{d}_j\right\|^{-\alpha} r^\alpha\right] = \frac{\pi\lambda_b}{\alpha-2}D^{2-\alpha}$. Based on (21), we simplify the antenna allocation optimization by reformulating the objective from maximizing the expected spectral efficiency to maximizing the expected SIR, thereby streamlining the analysis. Then, it follows that

$$\mathrm{E}_{r,\Phi_b^S,g_i}\left[\ln\left(1+\frac{S}{I}\right)\right] \approx \mathrm{E}_r\left[\ln\left(1+\overline{\mathrm{SIR}}\right)\right], \tag{22}$$

where $\overline{\mathrm{SIR}} = M_\mathrm{t}\left(\left(\frac{\alpha-2}{\pi\lambda_b}r^{-\alpha}+r^{-\alpha+2}\right)D^{\alpha-2}-1\right)$. In (22), we consider the optimal communication design, where the beamforming gain is M_t rather than $p^c(M_\mathrm{t}-1)$. The $\overline{\mathrm{SIR}}$ value increases monotonically with the size of cooperative regions D. Due to the complicated integral operation of the distance distribution r in (22), it is challenging to directly obtain the optimal antenna-to-BS allocation strategy based on (22). Thus, we analyze the relationship between the optimal number of antennas M_t and the expected SIR of the typical communication user. In the following, we use an approximate method for analysis, where a sufficiently small value of ϵ is chosen as the lower limit of integration to ensure the feasibility of the integral and the validity of the analysis.

$$\begin{aligned}&\mathrm{E}_r\left[\frac{\bar{S}_r}{\bar{I}_r}\right] = \int_\epsilon^D M_\mathrm{t}\left(\frac{\frac{\alpha-2}{\pi\lambda_b}r^{-\alpha}+r^{-\alpha+2}}{D^{-\alpha+2}}-1\right)f_r(r)dr \\ &= M_\mathrm{t}\Bigg(\frac{\alpha-2}{D^{-\alpha+2}}(\pi\lambda_b)^{\frac{\alpha-2}{2}}\int_\epsilon^{\pi\lambda_b D^2} u^{-\frac{\alpha}{2}}e^{-u}du \\ &+\frac{(\pi\lambda_b)^{\frac{\alpha-2}{2}}}{D^{-\alpha+2}}\int_\epsilon^{\pi\lambda_b D^2} u^{\frac{-\alpha+2}{2}}e^{-u}du + e^{-\pi\lambda_b D^2}-1\Bigg) \triangleq G(M_\mathrm{t}).\end{aligned} \tag{23}$$

Building on the above analysis, in the following, we investigate the optimal antenna-to-BS allocation in two specific cases.

Proposition 1: When $\alpha \to 2$, the optimal antenna-to-BS allocation strategy for communication is centralized, i.e., $\lambda_b^* = \frac{1}{\pi D^2}$ and $M_{\mathrm{t}}^* = \lambda_t \pi D^2$.

Proof: Let $\int_{\epsilon}^{\pi\lambda D^2} u^{-\frac{\alpha}{2}} e^{-u} du = \vartheta$. Upon substituting it into (23), due to $\lim_{\epsilon\to 0} \int_{\epsilon}^{\pi\lambda_b D^2} u^{\frac{-\alpha+2}{2}} e^{-u} du = \gamma\left(1, \pi\lambda_b D^2\right)$, it follows that

$$\mathrm{E}\left[\frac{\bar{S}_r}{\bar{I}_r}\right] = M_{\mathrm{t}}\left(\vartheta + \gamma\left(1, \pi\lambda_b D^2\right) + e^{-\pi\lambda_b D^2} - 1\right). \quad (24)$$

Due to $\gamma(1,x) = 1 - e^{-x}$, $\mathrm{E}\left[\frac{\bar{S}_r}{\bar{I}_r}\right] = M_{\mathrm{t}}\vartheta$, we have $\vartheta > 0$ since $\mathrm{E}\left[\frac{\bar{S}_r}{\bar{I}_r}\right] \geq 0$. Therefore, the derivative of $G(M_{\mathrm{t}})$ follows

$$G'(M_{\mathrm{t}}) = \frac{\vartheta}{2} \geq 0. \quad (25)$$

Thus, given a region $|\mathcal{A}|$, the number of antennas is $|\mathcal{A}| \times \lambda_t$, and the expected SIR of the communication user increases upon increasing the number of antennas allocated at each location. Therefore, the optimal antenna-to-BS allocation strategy is centralized, i.e., $\lambda_b^* = \frac{1}{\pi D^2}$ and $M_{\mathrm{t}}^* = \lambda_t \pi D^2$. ■

Proposition 2: When $\alpha \gg 4$, the optimal antenna-to-BS allocation strategy for communication is distributed, i.e., $\lambda_b^* = \lambda_t$, $M_{\mathrm{t}}^* = 1$.

Proof: In (23), we have $\int_{\epsilon}^{\pi\lambda D^2} u^{-\frac{\alpha}{2}} e^{-u} du \approx \frac{2\epsilon^{-\frac{\alpha}{2}+1}}{\alpha-2}$ and $\int_{\epsilon}^{\pi\lambda D^2} u^{\frac{-\alpha+2}{2}} e^{-u} du \approx \frac{2\epsilon^{\frac{-\alpha+4}{2}}}{\alpha-4}$. Then, it follows that

$$G(M_{\mathrm{t}}) = M_{\mathrm{t}}\left(C_0 M_{\mathrm{t}}^{\frac{2-\alpha}{2}} + e^{-\frac{\pi\lambda_t D^2}{M_{\mathrm{t}}}} - 1\right), \quad (26)$$

where $C_0 = \frac{2}{D^{-\alpha+2}}(\pi\lambda_t)^{\frac{\alpha-2}{2}} \epsilon^{-\frac{\alpha}{2}+1}\left(1 + \frac{\epsilon}{\alpha-4}\right)$. Due to $\int_{\epsilon}^{\frac{\pi\lambda_t D^2}{M_{\mathrm{t}}}} u^{-\frac{\alpha}{2}} e^{-u} du \geq \frac{2\epsilon^{-\frac{\alpha}{2}+1}}{\alpha-2}$, the derivative of $G(M_{\mathrm{t}})$ becomes as follows

$$G'(M_{\mathrm{t}}) = \left(2\left(\frac{\pi\lambda_t D^2}{M_{\mathrm{t}}}\right)^{\frac{\alpha-4}{2}} \epsilon^{-\frac{\alpha}{2}+1}\left(1 + \frac{\epsilon}{\alpha-4}\right)\frac{4-\alpha}{2} + 1\right) \times \frac{\pi\lambda_t D^2}{M_{\mathrm{t}}} \leq 0. \quad (27)$$

The inequality in (27) holds due to $2\left(\frac{\pi\lambda_t D^2}{M_{\mathrm{t}}}\right)^{\frac{\alpha-4}{2}} \epsilon^{-\frac{\alpha}{2}+1}\left(1 + \frac{\epsilon}{\alpha-4}\right)\frac{4-\alpha}{2} \ll -1$ when $\alpha \gg 4$. Therefore, $G(M_{\mathrm{t}})$ increases, as M_{t} decreases. ■

The above conclusions provide practical guidance for antenna-to-BS allocation. In environments suffering from strong fading, a distributed antenna allocation strategy should be adopted for positioning service antennas closer to the users. In such scenarios, the distributed antenna allocation enhances the useful signal, because although the interference may be increased, the resulting mitigation of fading is typically more substantial. Conversely, in environments having mild fading, such as line-of-sight-dominant channels, distributed allocation may significantly amplify the interference and this is not outweighed by the fading mitigation. In these cases, a centralized allocation can be more effective, as beamforming techniques can be used to strengthen the desired signal, while reducing interference.

V. Sensing and Communication Tradeoffs

In this section, we analyze the optimization of cooperative ISAC networks to demonstrate that antenna-to-BS allocation introduces a new degree of freedom, enabling a flexible balance between sensing and communication performance. Based on the derivations in Sections III and IV, the derived tractable performance expressions of both S&C are functions of the number of antennas and BS density. Then, we present a performance metric, namely the rate-CRLB performance region, to verify the effectiveness of the proposed cooperative ISAC schemes. Without loss of generality, the S-C network performance region is defined as

$$\mathcal{C}_{c-s}(L, N, p^c, p^s) = \Big\{(\hat{r}_c, \hat{\mathrm{crlb}}) : \hat{r}_c \leq R_c, \hat{\mathrm{crlb}} \geq \mathrm{CRLB}, p^s + p^c \leq 1, M_{\mathrm{t}}\lambda_b \leq \lambda_t, M_{\mathrm{r}}\lambda_b \leq \lambda_r\Big\}, \quad (28)$$

where $(\hat{r}_c, \hat{\mathrm{crlb}})$ represents an achievable rate-CRLB performance pair. By examining this region, we gain a clear view of how improvements in one domain (e.g., increasing communication rate) may impact the other (e.g., localization accuracy) and vice versa. In this case, the rate-CRLB performance region can be utilized to characterize all the achievable communication rate and achievable CRLB pairs under the constraint of the antenna resources.

VI. Simulations

Based on extensive numerical experiments, we investigated the core characteristics of ISAC networks and confirmed that our tractable expressions closely match the outcomes of Monte Carlo simulations. In our study, simulation results were averaged over various network configurations and small-scale fading scenarios. The system parameters include: $M_{\mathrm{t}} = 4$ transmit antennas, $M_{\mathrm{r}} = 10$ receive antennas, a per-BS transmit power of $P_{\mathrm{t}} = 1$ W, antenna densities $\lambda_t = \lambda_r = 50/\mathrm{km}^2$, an operating frequency of $f^c = 5$ GHz, a bandwidth $B \in [10, 100]$ MHz, a noise power of -100 dB, and pathloss exponents $\alpha = 4$ and $\beta = 2$.

In Fig. 2, both transmit and receive antenna densities are set to $50/\mathrm{km}^2$ with a noise level of $\sigma_s^2 = -100$ dB and a bandwidth of 10 MHz. In this figure, the legend distinguishes between a fixed energy allocation, denoted by P, which keeps each BS's total power constant regardless of the number of antennas, and a scenario where power scales with the number of transmit antennas, indicated by $M_{\mathrm{t}} \cdot P$. Under the fixed power constraint P, our analysis shows that a fully distributed configuration is optimal for TOF-based localization scheme. In contrast, the AOA-based method benefits from concentrating antennas to enhance angle estimation accuracy, with an optimal deployment of eight BSs per square kilometer. When the power scales with the number of antennas $M_{\mathrm{t}} \cdot P$, TOF-based approach favor a mixed configuration that blends centralized and distributed allocations, thereby balancing the beamforming gains with macro-diversity benefits.

Fig. 3 illustrates that an increase in the attenuation coefficient α makes a distributed allocation more advantageous.

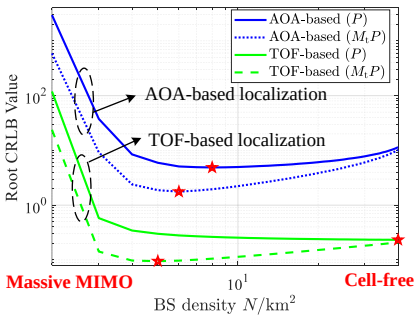

Fig. 2. Localization performance comparisons with respect to the cooperative BS density.

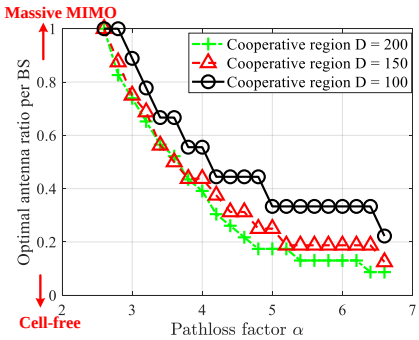

Fig. 3. Antenna allocation vs. path loss factor α with various radius D = 100, 150, 200 m.

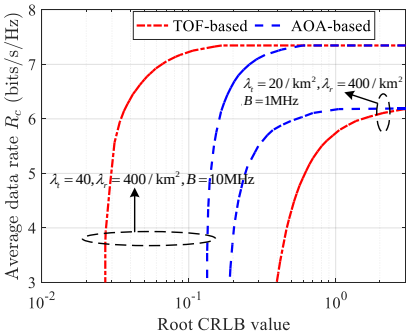

Fig. 4. Rate-CRLB performance boundary with different localization methods.

This occurs because distributing the antennas minimizes the average distance between service BSs and users, effectively diminishing interference from distant sources as both useful and interfering signals weaken over longer distances. On the other hand, when α is lower, centralized allocation becomes preferable since interference from remote BSs has a larger impact; despite the increased distance between BSs and users, the lower attenuation allows sufficient signal strength to be maintained. In Fig. 3, an optimal antenna ratio per BS of 1 indicates a massive MIMO configuration. Conversely, when this ratio approaches 0, the system effectively functions as a cell-free network. Moreover, as the cooperative area radius D expands (for instance, from 100 m to 200 m), the optimal fraction of antennas deployed at each BS relative to the total in the area decreases, reflecting the need for a denser antenna distribution near users to sustain high communication rates in larger cooperation zones.

Fig. 4 presents the performance boundaries defined in (28) for optimal joint and power allocation across two localization schemes, with a cooperation radius $D = 1000$ m. Notably, the both TOF-based and AOA-based localization methods, significantly extends the performance frontier. Furthermore, overall sensing and communication performance improves with an increasing transmit antenna density, due to enhanced flexibility in resource allocation that boosts beamforming gains. As the bandwidth decreases, the performance of AOA-based localization becomes superior to that of TOF-based methods, primarily because the accuracy of TOF measurements deteriorates with reduced bandwidth.

VII. Conclusions

This research introduces a novel cooperative ISAC network that integrates multi-static sensing with CoMP data transmission, utilizing advanced localization techniques based on AOA and TOF metrics. We show that an optimal antenna-to-BS assignment, achieved by balancing centralized and distributed configurations, substantially boosts network performance through improved spatial diversity and coherent processing gains. Furthermore, our analysis reveals the scaling laws of various localization methods and presents a robust framework for assessing communication data rates under different allocation schemes.

References

[1] K. Meng, Q. Wu, W. Chen, and D. Li, "Sensing-assisted communication in vehicular networks with intelligent surface," *IEEE Trans. Veh. Technol.*, vol. 73, no. 1, pp. 876–893, 2024.

[2] Y. Cui, F. Liu, X. Jing, and J. Mu, "Integrating sensing and communications for ubiquitous IoT: Applications, trends, and challenges," *IEEE Net.*, vol. 35, no. 5, pp. 158–167, Sep./Oct. 2021.

[3] K. Meng *et al.*, "Cooperative ISAC networks: Opportunities and challenges," *IEEE Wireless Communications*, pp. 1–8, 2024.

[4] F. De Saint Moulin, C. Wiame, C. Oestges, and L. Vandendorpe, "Cooperative sensing in automotive urban scenarios using poisson line processes," in *2023 31st EUSIPCO*, 2023, pp. 720–724.

[5] K. Hosseini, W. Yu, and R. S. Adve, "A stochastic analysis of network MIMO systems," *IEEE Trans. Signal Process.*, vol. 64, no. 16, pp. 4113–4126, Aug. 2016.

[6] K. Meng, C. Masouros, A. P. Petropulu, and L. Hanzo, "Cooperative ISAC networks: Performance analysis, scaling laws and optimization," *IEEE Trans. Wireless Commun.*, vol. 24, no. 2, pp. 877–892, 2025.

[7] A. Salem *et al.*, "Rethinking dense cells for integrated sensing and communications: A stochastic geometric view," *IEEE Open J. Commun. Society*, vol. 5, pp. 2226–2239, 2024.

[8] T. S. Rappaport, Y. Xing, G. R. MacCartney, A. F. Molisch, E. Mellios, and J. Zhang, "Overview of millimeter wave communications for fifth-generation (5G) wireless networks-with a focus on propagation models," *IEEE Trans. Antennas Propag.*, vol. 65, no. 12, pp. 6213–6230, 2017.

[9] H. Q. Ngo, A. Ashikhmin, H. Yang, E. G. Larsson, and T. L. Marzetta, "Cell-free massive MIMO versus small cells," *IEEE Trans. Wireless Commun.*, vol. 16, no. 3, pp. 1834–1850, 2017.

[10] W. Cai *et al.*, "Deployment optimization of uniform linear antenna arrays for a two-path millimeter wave communication system," *IEEE Commun. Lett.*, vol. 19, no. 4, pp. 669–672, 2015.

[11] J. Li and P. Stoica, *MIMO radar signal processing*. John Wiley & Sons, 2008.

[12] P. Stoica and A. Nehorai, "MUSIC, maximum likelihood, and Cramer-rao bound," *IEEE Trans. Acoust., Speech, Signal Processing*, vol. 37, no. 5, pp. 720–741, 1989.

[13] J. Li and R. Compton, "Maximum likelihood angle estimation for signals with known waveforms," *IEEE Trans. Signal Process.*, vol. 41, no. 9, pp. 2850–2862, 1993.

[14] M. A. Richards *et al.*, *Fundamentals of radar signal processing*. Mcgraw-hill New York, 2005, vol. 1.

[15] A. Liu *et al.*, "A survey on fundamental limits of integrated sensing and communication," *IEEE Commun. Surveys Tuts.*, vol. 24, no. 2, pp. 994–1034, Nov. 2022.

[16] M. Sadeghi, F. Behnia, R. Amiri, and A. Farina, "Target localization geometry gain in distributed MIMO radar," *IEEE Trans. Signal Process.*, vol. 69, pp. 1642–1652, 2021.

[17] J. Park, N. Lee, J. G. Andrews, and R. W. Heath, "On the optimal feedback rate in interference-limited multi-antenna cellular systems," *IEEE Trans. Wireless Commun.*, vol. 15, no. 8, pp. 5748–5762, Aug. 2016.